The $Al^+ - H_2$ cation complex: Rotationally resolved infrared spectrum, potential energy surface, and rovibrational calculations

C. Emmeluth, B. L. J. Poad, C. D. Thompson, G. Weddle, E. J. Bieske, A. A. Buchachenko, T. A. Grinev, and J. Kłos

Citation: The Journal of Chemical Physics **127**, 164310 (2007);
View online: https://doi.org/10.1063/1.2778422
View Table of Contents: http://aip.scitation.org/toc/jcp/127/16
Published by the American Institute of Physics

The Al^+-H_2 cation complex: Rotationally resolved infrared spectrum, potential energy surface, and rovibrational calculations

C. Emmeluth, B. L. J. Poad, C. D. Thompson, G. Weddle,[a] and E. J. Bieske[b]
School of Chemistry, University of Melbourne, Melbourne 3010, Australia

A. A. Buchachenko[c] and T. A. Grinev
Laboratory of Molecular Structure and Quantum Mechanics, Department of Chemistry, Moscow State University, Moscow 119992, Russia

J. Kłos
Department of Chemistry and Biochemistry, University of Maryland, College Park, Maryland 20742-2021, USA

(Received 13 July 2007; accepted 7 August 2007; published online 25 October 2007)

The infrared spectrum of the Al^+-H_2 complex is recorded in the H–H stretch region (4075–4110 cm^{-1}) by monitoring Al^+ photofragments. The H–H stretch band is centered at 4095.2 cm^{-1}, a shift of −66.0 cm^{-1} from the $Q_1(0)$ transition of the free H_2 molecule. Altogether, 47 rovibrational transitions belonging to the parallel K_a=0-0 and 1-1 subbands were identified and fitted using a Watson *A*-reduced Hamiltonian, yielding effective spectroscopic constants. The results suggest that Al^+-H_2 has a T-shaped equilibrium configuration with the Al^+ ion attached to a slightly perturbed H_2 molecule, but that large-amplitude intermolecular vibrational motions significantly influence the rotational constants derived from an asymmetric rotor analysis. The vibrationally averaged intermolecular separation in the ground vibrational state is estimated as 3.03 Å, decreasing by 0.03 Å when the H_2 subunit is vibrationally excited. A three-dimensional potential energy surface for Al^+-H_2 is calculated *ab initio* using the coupled cluster CCSD(T) method and employed for variational calculations of the rovibrational energy levels and wave functions. Effective dissociation energies for Al^+-H_2(para) and Al^+-H_2(ortho) are predicted, respectively, to be 469.4 and 506.4 cm^{-1}, in good agreement with previous measurements. The calculations reproduce the experimental H–H stretch frequency to within 3.75 cm^{-1}, and the calculated *B* and *C* rotational constants to within ~2%. Agreement between experiment and theory supports both the accuracy of the *ab initio* potential energy surface and the interpretation of the measured spectrum. © *2007 American Institute of Physics*. [DOI: 10.1063/1.2778422]

I. INTRODUCTION

Interactions between molecules and metal cations play a key role in a variety of chemical contexts including catalysis, enzymes, and hydrogen storage in porous materials. Experimentally, perhaps the most direct way of probing these interactions is by spectroscopically studying complexes consisting of a single molecule attached to a metal cation, ideally in the gas phase. The spectroscopic data can be compared with corresponding theoretical data derived from rovibrational calculations using an *ab initio* potential energy surface (PES). In the current study we implement this combined approach to characterize the Al^+-H_2 complex. The simplicity of the triatomic system facilitates detailed comparison between experiment and theory and enables key aspects of the $Al^+ + H_2$ interaction to be examined. The spectroscopic work complements recent infrared investigations of clusters composed of simple metal cations such as Li^+, Na^+, K^+, Mg^+, Ca^+, and Al^+ "solvated" by small molecules such as H_2O, NH_3, and CO_2.[1–8] Structural information for these species has mainly been derived from vibrationally resolved infrared spectra, or spectra containing partially resolved rotational features, interpreted in conjunction with theoretical predictions for the vibrational frequencies and intensities for lower energy isomers.

There have been several earlier studies of the Al^+-H_2 complex and related systems. Kemper *et al.* established dissociation energies for the Al^+-H_2 and $Al^+-(H_2)_2$ complexes of 470±50 and 385±50 cm^{-1} through measurements of the clustering equilibrium constants for the $Al^+-(H_2)_{n-1} + H_2 \rightleftarrows Al^+-(H_2)_n$ reactions.[9] Several theoretical studies have addressed the equilibrium structures, vibrational frequencies, and binding energies of the $Al^+-(H_2)_n$ clusters, confirming that they consist essentially of intact hydrogen molecules attached by relatively weak bonds to the Al^+ core.[9–11] Due to the long-range charge-quadrupole interaction, the Al^+-H_2 complex preferentially adopts a T-shaped structure, a bonding motif that is preserved in the larger $Al^+-(H_2)_n$ clusters.[9,10]

One important aspect of the theoretical studies has been investigation of σ bond activation and formation of the inserted $HAlH^+$ species. Sharp *et al.* found that the electrostatically bound Al^+-H_2 complex lies 13.1 kcal/mol lower in

[a]Also at Department of Chemistry, Fairfield University, Connecticut.
[b]Electronic mail: evanjb@unimelb.edu.au
[c]Electronic mail: alexei@classic.chem.msu.su

energy than the inserted $HAlH^+$ structure.[10] Conversion of the Al^+-H_2 complex to the inserted $HAlH^+$ form is predicted to proceed by breaking first the H_2 bond, followed by consecutive formation of two equivalent AlH bonds with a calculated activation energy of 85.0 kcal/mol.[10] The corresponding reaction for the isovalent B^+ ion, where the inserted HBH^+ form is 55.9 kcal/mol more stable than the B^+-H_2 complex, was found to be expedited in $B^+-(H_2)_n$ clusters, with a significant lowering in the insertion barrier for $n=3$ compared to $n=1$ (3 kcal/mol vs 56 kcal/mol).[12,13] Although the insertion barrier is also predicted to be lowered for the larger $Al^+-(H_2)_n$ clusters, it remains appreciable (53.2 kcal/mol for $n=3$).[10]

Related experimental[14] and theoretical[15–18] studies have focused on the $Al^+(^1S)+H_2(^1\Sigma_g^+)\rightarrow AlH^+(^2\Sigma^+)+H(^2S)$ reaction which is 3.98 eV endothermic. One unusual feature of the reaction is an exceptionally low energetic threshold for AlD^+ production from collisions between $Al^+(^1S)$ and HD compared to the threshold for AlH^+ production.

In this paper we report a fully rotationally resolved infrared spectrum of the Al^+-H_2 complex. The spectroscopic data allow us to characterize the structure of the complex and its predissociation dynamics. The experimental work is complemented by a theoretical characterization of the complex. A full three-dimensional PES for Al^+-H_2 was computed *ab initio* using the coupled cluster CCSD(T) method and used for variational rovibrational calculations to derive theoretical information that is directly comparable with the measured spectroscopic data. A similar approach was successfully employed for characterizing the halide-H_2 anion complexes.[19–21] Large amplitude vibrational motions are expected to play a significant role in the Al^+-H_2 complex because of the weak nature of the interaction and low mass of the H atom constituents. For this reason it is necessary to go beyond the harmonic oscillator/rigid rotor approximation to describe the rovibrational energy levels. This was found to be the case for the Li^+-H_2 and Li^+-D_2 complexes which have also been characterized spectroscopically[22,23] and theoretically.[24–27]

II. EXPERIMENTAL METHODS

The infrared spectrum of Al^+-H_2 was obtained in the H–H stretch vibration by monitoring Al^+ fragments while scanning the IR wavelength. The Al^+-H_2 complexes were produced in a supersonic expansion of H_2 (8 bars) passed over a laser-ablated Al rod. The translating and rotating rod was irradiated with the fundamental (1064 nm, 7 mJ/pulse), doubled (532 nm, 3 mJ/pulse), and quadrupled (266 nm, 1 mJ/pulse) outputs of a pulsed Nd:YAG (yttrium aluminum garnet) laser running at 20 Hz. The desired Al^+-H_2 ions were selected by a quadrupole mass filter and deflected through 90° by a quadrupole bender into an octopole ion guide where they were overlapped by the counterpropagating output of a tunable IR source (Continuum Mirage 3000, 0.017 cm^{-1} bandwidth). Resulting photofragments were selected by a second quadrupole mass filter and detected using a microchannel plate coupled to a scintillator and a photomultiplier tube.

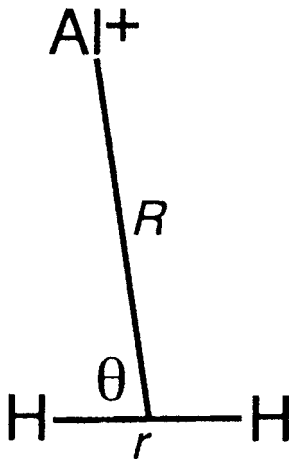

FIG. 1. Jacobi coordinates for the Al^+-H_2 complex.

The wavelength of the IR light was determined by measuring the wavelengths of the signal output from the first stage of the optical parametric oscillator (OPO) and the 532 nm pump beam of the seeded Nd:YAG laser using a wavemeter (HighFinesse WS/7). Transition wave numbers were corrected for the Doppler shift resulting from the ions' 10 eV translational energy in the octopole ion guide. The absolute uncertainty of the line wave numbers is decided by the uncertainty of the ion energy in the octopole ion guide and is estimated as ±0.10 cm^{-1}. The relative uncertainties of the lines' wave numbers are estimated as ±0.01 cm^{-1}. The lines' intensities were not normalized for laser power or parent ion signal intensity. Further details of the experimental apparatus can be found in Refs. 22 and 28.

III. THEORETICAL METHODS

A. Three-dimensional potential energy surface for Al^+-H_2

The three-dimensional ground state PES for Al^+-H_2 was calculated *ab initio* using the MOLPRO program suite.[29] The augmented correlation-consistent aug-cc-pVQZ (AVQZ) atomic basis sets[30,31] for the Al and H atoms were supplemented by the $3s3p2d2f1g$ bond function set[32] placed at the midpoint of the R vector joining the H_2 center of mass and the Al ion. The restricted Hartree-Fock method was used to generate molecular orbitals for the subsequent coupled cluster with single and double excitations and noniterative correction to triple excitations CCSD(T) calculations.[33–35] The interaction energy was calculated by the supermolecular approach which implements the Boys-Bernardi correction to the basis set superposition error.[36] During calculations the $1s$ core orbital of Al was kept frozen. Electronic structure calculations were performed on a discrete grid of Jacobi coordinates (r, R, θ—see Fig. 1) consisting of 6 points in the H_2 internuclear distance (r from $1.0a_0$ to $2.2a_0$), 40 points in the intermonomer coordinate (R from $2.75a_0$ to $40.0a_0$), and four values of angle θ between the r and R vectors (0°, 30°, 60°, and 90°).

The analytical form of the PES uses a spline in the R coordinate, a fourth-order even Legendre polynomial expan-

sion over the angle θ, and a fifth-order power series expansion in the dimensionless coordinate $x=(r-r_e)/r_e$ as described in Ref. 19. The *ab initio* interaction energies were cubic splined in the R coordinate for each combination of θ and r on the grid and further expanded in a series of Legendre polynomials and a power series in x to account for the H_2 stretch coordinate. The range and number of points in the R variable covered in the *ab initio* calculations was sufficient to justify using a spline in dynamical calculations. The FORTRAN subroutine for generating the analytical PES is available as supplementary material.[37]

B. Dynamical calculations

The *ab initio* Al^+-H_2 PES was used for both full three-dimensional (3D) and two-dimensional (2D) rovibrational calculations. The 3D rovibrational calculations for $n_{HH}=0$, $J=0-4$ levels were undertaken using the TRIATOM program[38] utilizing a basis set comprising 8 Morse functions in the H–H stretch, 14 Morse functions in the intermolecular stretch, and 10 Legendre functions for the angular coordinate. The masses of the Al and H atoms were taken as 26.981 539 and 1.007 825 amu, respectively.

The rovibrational energy levels were also calculated within the 2D diabatic approximation as described in Ref. 19. In brief, the total PES E_{tot} was segregated into the sum of the interaction energy E_{int} and the unperturbed H_2 potential. The effective 2D potential energy surfaces for $Al^+ + H_2(n_{HH}=0)$ and $Al^+ + H_2(n_{HH}=1)$ were obtained by averaging the PES over the respective H_2 vibrational wave functions. The resulting 2D problem was solved variationally using the symmetry-adapted angular basis set[39,40] that splits the total Hamiltonian matrix into four $J^{p_i p_j}$ blocks defined by the total end-over-end angular momentum J, inversion parity $p=(-1)^J p_i$, and the parity with respect to permutation of H nuclei, p_j. The $p_j=+1$ and $p_j=-1$ levels correspond to Al^+ interacting with para- and ortho-H_2, respectively.

Using the 2D approach the five lowest rovibrational energy levels for $Al^+ + H_2(n_{HH}=0)$ and $Al^+ + H_2(n_{HH}=1)$ were computed for each $J^{p_i p_j}$ symmetry block with $J \leqslant 8$. The levels were assigned using the nomenclature for a rigid asymmetric top ($J_{K_a K_c}$) using the correlation scheme described by Reid *et al.*,[40] and to the number of quanta in the H_2 stretch mode (n_{HH}) and in the intermolecular stretching and bending vibrational modes (n_s and n_b, respectively). Using the full 3D approach, the lowest two or three rovibrational energy levels were computed for each symmetry block with $J \leqslant 4$. Note that the 3D calculations are restricted to $n_{HH}=0$. A list of the computed 2D and 3D levels together with their assignments is provided as supplementary material.[37]

IV. RESULTS AND DISCUSSION

A. *Ab initio* PES and energy levels

The main features of the $Al^+ + H_2$ interaction are apparent in Fig. 2, where the potential energy is displayed as a contour plot in Cartesian coordinates for fixed H–H separation ($r=0.746$ Å). The form of the PES is determined primarily by the charge-quadrupole electrostatic interaction

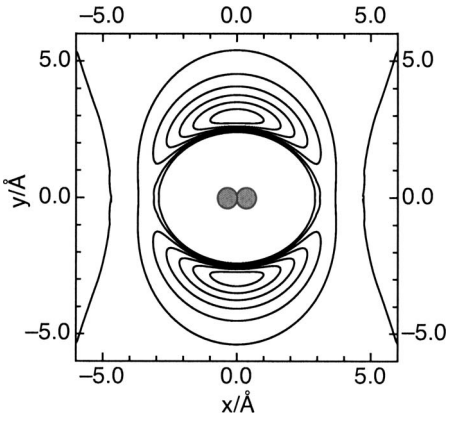

FIG. 2. Intermolecular PES for $Al^+ + H_2$ for fixed H–H separation ($r=0.746$ Å). Contour spacing is 100 cm^{-1}. The potential minimum in the T-shaped configuration lies −668.4 cm^{-1} below the dissociation asymptote.

(strongly anisotropic) and charge-induced dipole induction interaction (weakly anisotropic).[16] As a result, the global minimum of the PES corresponds to a T-shaped configuration where the electrostatic interaction is most attractive. The linear geometry, where the charge-quadrupole interaction is repulsive, corresponds to a saddle point and barrier to H_2 internal rotation. Presented in Table I are the locations and energies of stationary points at selected H–H distances (0.741 Å—equilibrium distance of the free H_2 molecule, 0.746 Å—minimum of the Al^+-H_2 PES, and 0.766 and 0.818 Å—vibrationally averaged distances of H_2 for $n_{HH}=0$ and 1, respectively). The interaction energy E_{int} decreases as the r coordinate increases and as a result the equilibrium H–H bond length for the total PES E_{tot} is 0.005 Å larger than for the free H_2 molecule. The increase in the interaction strength with r implies a redshift of the vibrational transitions of H_2 upon the complexation with Al^+.

The equilibrium structural parameters for the PES ($r_e=0.746$ Å, $R_e=2.957$ Å, and $D_e=668.4$ cm^{-1}) are comparable with previous MP2/aug-cc-pVTZ results reported in Ref. 10 ($r_e=0.742$ Å, $R_e=3.011$ Å, and $D_e=612.1$ cm^{-1}), and CCSD(T)/cc-pVTZ results from Ref. 11 ($r_e=0.747$ Å and $R_e=2.990$ Å).

Table II summarizes the properties of the Al^+-H_2 complex determined through the 2D and 3D rovibrational calculations using the new CCSD(T) PES. For $n_{HH}=0$, the 2D and 3D approaches give very similar values for the dissociation energy and intermolecular stretch and bend vibrational frequencies. The 2D and 3D energies for the higher J levels of the $n_{HH}=0$ manifold are also very close (the energies are

TABLE I. Equilibrium distances R_e (Å), and total E_{tot} and interaction E_{int} energies (cm^{-1}) for Al^+-H_2 at selected H–H distances r. Energy is with respect to the $Al^+ + H_2(r_e)$ limit.

r (Å)	Minimum ($\theta=\pi/2$)			Saddle ($\theta=0$)		
	R_e	E_{tot}	E_{int}	R_e	E_{tot}	E_{int}
0.741	2.960	−664.3	−664.3	3.340	−133.5	−133.5
0.746	2.957	−668.4	−671.3	3.338	−132.1	−135.0
0.766	2.947	−613.5	−699.0	3.329	−55.8	−141.3
0.818	2.924	−53.8	−769.6	3.304	+555.6	−160.3

TABLE II. Calculated properties of the Al^+-H_2 complex based on the CCSD(T) PES and 3D and 2D rovibrational calculations. Constants with double prime correspond to the ground $n_{HH}=0$ state, with the single prime—to the excited $n_{HH}=1$ sate. Also listed are calculated results from Refs. 10 and 11.

	3D	2D	Ref. 10	Ref. 11
r_e (Å)	0.746		0.742	0.747
R_e (Å)	2.957		3.011	2.990
D_e (Å)	668.4		612.1	
ν_s'' (cm^{-1})	153.6	152.9		
ν_b'' (cm^{-1})	282.6	282.8		
D_o'' (cm^{-1})	472.5	469.4		
ν_s' (cm^{-1})		162.9		
ν_b' (cm^{-1})		287.8		
D_o' (cm^{-1})		531.6		

provided as supplementary material[37]). In what follows, we mainly focus on the 2D results to facilitate comparisons between Al^+-H_2 in the $n_{HH}=0$ and $n_{HH}=1$ states.

There are essentially two noninterconverting forms of the complex corresponding to either para- or ortho-H_2 attached to the Al^+ ion. The ground state of the system ($n_{HH}=0$, $n_s=0$, $n_b=0$, and $J_{K_aK_c}=0_{00}$) corresponds to Al^+-H_2 (para) and has a computed dissociation energy of 469.4 cm^{-1} (2D). The lowest state of Al^+-H_2 (ortho) ($n_{HH}=0$, $n_s=0$, $n_b=0$, and $J_{K_aK_c}=1_{11}$) lies above the ground state by 81.7 cm^{-1} (2D). The effective dissociation energy of Al^+-H_2 (ortho), which fragments to $Al^++H_2(j=1)$, is 506.4 cm^{-1} (2D), ~37 cm^{-1} greater than the dissociation energy of Al^+-H_2 (para). The calculated binding energies for both the Al^+-H_2 (para) and Al^+-H_2 (ortho) forms agree very well with values obtained from equilibrium clustering experiments ($D_0=470\pm50$ cm^{-1}; Ref. 9). As discussed below, the greater effective stability of complexes containing ortho-H_2 has a pronounced effect on the Al^+-H_2 IR spectrum.

B. Infrared spectrum of Al^+-H_2

The infrared spectrum of Al^+-H_2 in the H–H stretch region (4075–4110 cm^{-1}) is shown in Fig. 3. Because the transition moment associated with excitation of the H–H stretch lies along the intermolecular bond, one expects an *A*-type band, consisting of overlapping K_a=0-0, 1-1, 2-2, etc., subbands ($\Delta K_a=0$, $\Delta J=0$, ±1 selection rules). Altogether 50 transitions were identified. Of these, 13 lines are assigned to K_a=0-0 transitions, 34 lines to K_a=1-1 transitions (*P* branch: 14 lines, *Q* branch: 6 lines, *R* branch: 14 lines), and 3 lines to K_a=2-2 transitions. Wave numbers for the transitions are listed in Table III.

Asymmetry doublets are resolved in the *P* and *R* branches of the K_a=1-1 subband (see Fig. 3). In contrast, the three K_a=2-2 *R*-branch lines appear as single peaks according to the expected reduction in asymmetry splitting for the higher K_a levels; for $J\leqslant 8$ the splittings of the K_a=2-2 transitions are predicted to be <0.02 cm^{-1}.

Table III lists differences between the experimental line positions and computed transition energies determined through 2D rovibrational calculations for $Al^+-H_2(n_{HH}=0)$ and $Al^+-H_2(n_{HH}=1)$. Generally, agreement between experiment and theory is very good; the calculations systematically overestimate the positions of the lower *J* lines by ~3.75 cm^{-1} with slightly smaller deviations for higher *R*-branch lines and slightly larger deviations for higher *P*-branch lines. Up to $J=8$ the difference does not exceed 4 cm^{-1} and varies within a narrow interval of 3.75 ± 0.4 cm^{-1}.

A conspicuous feature of the infrared spectrum is that the K_a=1-1 lines (associated with complexes containing ortho-H_2) are much more intense than the K_a=0-0 lines (associated with complexes containing para-H_2). The intensity ratio (around 9:1) is considerably greater than expected given the 3:1 ortho/para population ratio for natural H_2 gas. Preferential formation of complexes containing ortho-H_2 has been noted for a range of neutral and charged species.[41–43] The explanation is that ortho-H_2 is easier to orient in an electric field than para-H_2 so that the $Al^+\cdots H_2$ (ortho) bond is stronger than the $Al^+\cdots H_2$ (para) bond (510.6 compared to 472.5 cm^{-1} according to the 2D calculations described in Sec. IV A). Direct interconversion of Al^+-H_2 (para) to Al^+-H_2 (ortho) (and vice versa) should be extremely inefficient in the gas phase, although facile exchange of the attached H_2 ligand undoubtedly occurs in the initial part of the

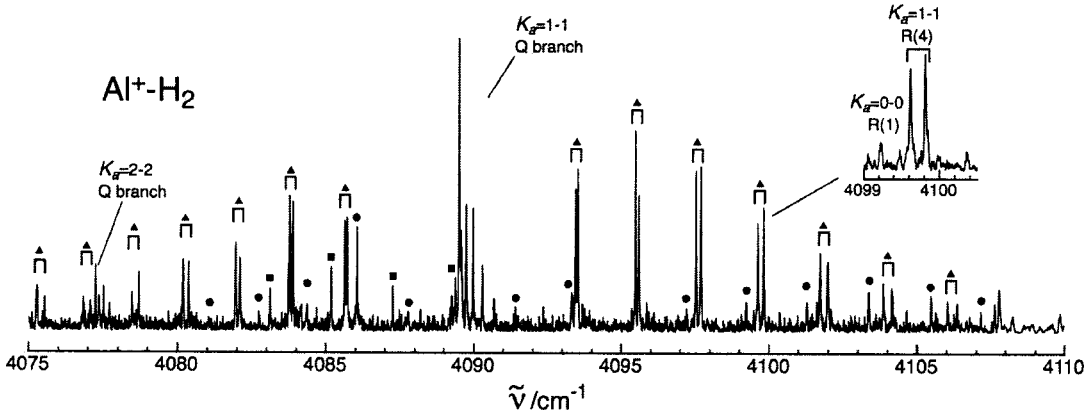

FIG. 3. Infrared spectrum of Al^+-H_2 in the H–H stretch region. The K_a=0-0 transitions are indicated by filled circles, K_a=1-1 transitions by triangles, and K_a=2-2 transitions by squares.

TABLE III. Measured transition wave numbers for Al^+-H_2. Given in parentheses is the difference (last significant figure) between the measured value and the value obtained using the fitted parameters listed in Table IV. Only K_a=0-0 and 1-1 lines were included in the fits. Differences between the experimental and theoretical values obtained from 2D rovibrational calculations (Sec. IV A) are given in square brackets.

R branch			*P* branch			*Q* branch		
Transition	Wave number		Transition	Wave number		Transition	Wave number	
				K_a=0-0				
$1_{0,1}\leftarrow 0_{0,0}$	4097.22(1)	[−3.70]	$0_{0,0}\leftarrow 1_{0,1}$	⋯	⋯			
$2_{0,2}\leftarrow 1_{0,1}$	4099.22(−1)	[−3.67]	$1_{0,1}\leftarrow 2_{0,2}$	4091.41(0)	[−3.82]			
$3_{0,3}\leftarrow 2_{0,2}$	4101.28(0)	[−3.62]	$2_{0,2}\leftarrow 3_{0,3}$	4089.87(0)	[−3.85]			
$4_{0,4}\leftarrow 3_{0,3}$	4103.37(1)	[−3.57]	$3_{0,3}\leftarrow 4_{0,4}$	4087.77(−1)	[−3.84]			
$5_{0,5}\leftarrow 4_{0,4}$	4105.47(−1)	[−3.55]	$4_{0,4}\leftarrow 5_{0,5}$	4086.05(1)	[−3.91]			
$6_{0,6}\leftarrow 5_{0,5}$	4107.63(0)	[−3.49]	$5_{0,5}\leftarrow 6_{0,6}$	4084.36(−1)	[−3.95]			
$7_{0,7}\leftarrow 6_{0,6}$	4109.82(1)	[−3.42]	$6_{0,6}\leftarrow 7_{0,7}$	4082.77(1)	[−3.96]			
				K_a=1-1				
$2_{1,2}\leftarrow 1_{1,1}$	4093.45(0)	[−3.61]	$1_{1,0}\leftarrow 2_{1,1}$	4085.63(−1)	[−3.78]	$1_{1,1}\leftarrow 1_{1,0}$	4089.50(0)	[−3.69]
$2_{1,1}\leftarrow 1_{1,0}$	4093.53(0)	[−3.61]	$1_{1,1}\leftarrow 2_{1,2}$	4085.72(1)	[−3.76]	$1_{1,0}\leftarrow 1_{1,1}$	4089.58(0)	[−3.69]
$3_{1,3}\leftarrow 2_{1,2}$	4095.47(0)	[−3.58]	$2_{1,1}\leftarrow 3_{1,2}$	4083.77(0)	[−3.81]	$2_{1,2}\leftarrow 2_{1,1}$	4089.50(0)	[−3.69]
$3_{1,2}\leftarrow 2_{1,1}$	4095.58(−1)	[−3.58]	$2_{1,2}\leftarrow 3_{1,3}$	4083.88(−1)	[−3.81]	$2_{1,1}\leftarrow 2_{1,2}$	4089.74(0)	[−3.69]
$4_{1,4}\leftarrow 3_{1,3}$	4097.53(0)	[−3.53]	$3_{1,2}\leftarrow 4_{1,3}$	4081.95(−1)	[−3.85]	$3_{1,3}\leftarrow 3_{1,2}$	⋯	⋯
$4_{1,3}\leftarrow 3_{1,2}$	4097.69(0)	[−3.53]	$3_{1,3}\leftarrow 4_{1,4}$	4082.12(1)	[−3.83]	$3_{1,2}\leftarrow 3_{1,3}$	4089.97(0)	[−3.69]
$5_{1,5}\leftarrow 4_{1,4}$	4099.62(1)	[−3.49]	$4_{1,3}\leftarrow 5_{1,4}$	4080.20(1)	[−3.87]	$4_{1,4}\leftarrow 4_{1,3}$	⋯	⋯
$5_{1,4}\leftarrow 4_{1,3}$	4099.81(0)	[−3.49]	$4_{1,3}\leftarrow 5_{1,5}$	4080.38(0)	[−3.88]	$4_{1,3}\leftarrow 4_{1,4}$	4090.30(1)	[−3.67]
$6_{1,6}\leftarrow 5_{1,5}$	4101.71(−1)	[−3.47]	$5_{1,4}\leftarrow 6_{1,5}$	4078.48(−1)	[−3.92]	$5_{1,5}\leftarrow 5_{1,4}$	⋯	⋯
$6_{1,5}\leftarrow 5_{1,4}$	4101.98(1)	[−3.43]	$5_{1,5}\leftarrow 6_{1,6}$	4078.71(0)	[−3.91]	$5_{1,4}\leftarrow 5_{1,5}$	4090.68(0)	[−3.68]
$7_{1,7}\leftarrow 6_{1,6}$	4103.87(1)	[−3.40]	$6_{1,5}\leftarrow 7_{1,6}$	4076.84(0)	[−3.95]			
$7_{1,6}\leftarrow 6_{1,5}$	4104.14(0)	[−3.40]	$6_{1,6}\leftarrow 7_{1,7}$	4077.09(−1)	[−3.95]			
$8_{1,8}\leftarrow 7_{1,7}$	4106.03(1)	[−3.36]	$7_{1,6}\leftarrow 8_{1,7}$	4075.28(1)	[−3.96]			
$8_{1,7}\leftarrow 7_{1,6}$	4106.35(−1)	[−3.36]	$7_{1,7}\leftarrow 8_{1,8}$	4075.54(−1)	[−3.98]			
				K_a=2-2				
$3_{2,2}\leftarrow 2_{2,1}$	4083.12	[−3.61]				maximum	4077.24	[3.75]
$3_{2,1}\leftarrow 2_{2,0}$	4083.12	[−3.61]						
$4_{2,3}\leftarrow 3_{2,2}$	4085.18	[−3.60]						
$4_{2,2}\leftarrow 3_{2,1}$	4085.18	[−3.60]						
$5_{2,4}\leftarrow 4_{2,3}$	4087.26	[−3.54]						
$5_{2,3}\leftarrow 4_{2,2}$	4087.26	[−3.54]						

supersonic expansion. Complexes containing the more strongly bound ortho-H_2 molecules are always favored in the ligand exchange equilibrium.[19,21,44]

C. Asymmetric rotor analysis

The K_a=0-0 and 1-1 transitions were fitted using an *A*-reduced Watson Hamiltonian; resulting parameters are listed in Table IV. Adjustable parameters included the ground and excited state *B* and *C* rotational constants, and distortion terms Δ_J and Δ_{JK}. It is not possible to determine A'' or A' through analysis of the parallel *A*-type transition; rather $\Delta A = A' - A''$ is ascertained. For the fits, A'' was constrained to 59.34 cm^{-1}, the rotational constant of free H_2 in its ground vibrational state;[45] note, however, that the fitted parameters are quite insensitive to the A'' value.

The four K_a=2-2 *R*-branch lines were not included in the total fit. However, their frequencies were used to estimate the position of the K_a=2-2 *Q* branch as 4077.1 cm^{-1}, close to a peak in the spectrum at 4077.2 cm^{-1} (marked in Fig. 3). If, as seems very likely, this assignment is correct, the 2D rovibrational calculations reproduce the *relative* positions of the K_a=0-0, 1-1, and 2-2 subband origins to within 0.1 cm^{-1}.

Table IV includes parameters resulting from fits to the calculated 2D (n_{HH}=0 and n_{HH}=1) and 3D (n_{HH}=0) energy levels. For fits to the calculated levels, *A* was also an adjustable parameter. By comparing the experimental and theoretical constants, it is apparent that the calculations underestimate $\bar{B}''$ and $\bar{B}'$ by ~2%, overestimate ΔA by ~1%, and predict the centrifugal distortion parameters to within experimental error.

The spectroscopic constants listed in Table IV can be used to estimate the ground and excited state intermolecular separations for Al^+-H_2. From $\bar{B}''$ and $\bar{B}'$ one can deduce vibrationally averaged $Al^+\cdots H_2$ intermolecular separations for the ground and excited states of 3.035 and 3.005 Å, respectively. Corresponding intermolecular separations extracted from the theoretical 2D $\bar{B}$ values are slightly longer (3.065 and 3.031 Å, respectively). The small overestimation of the intermolecular separation may be a result of the Boys-Bernardi counterpoise method overcompensating for the basis set superposition error (BSSE).

For a rigid, T-shaped, triatomic complex it would be pos-

TABLE IV. Constants for Al^+-H_2 obtained by fitting the K_a=0-0 and 1-1 transitions to a Watson *A*-reduced Hamiltonian. (Units for constants are cm^{-1}.) Parameters obtained by fitting the K_a=0-0 and 1-1 transition independently are given in the first two columns. The last two columns give parameters obtined by fitting energy levels derived from 2D and 3D rovibrational calculations (see Ref. 37 for the energies). For each value, the error in the last significant figure(s) is given in brackets.

	Expt.			Theory 2D	Theory 3D
	$K_a=0$	$K_a=1$	$K_a=0,1$	$K_a=0,1$	$K_a=0,1$
A''	⋯			80.813(7)	79.520(9)
B''	⋯	0.9867(10)	0.9867(10)	0.9680(6)	0.970(2)
C''	⋯	0.9484(10)	0.9483(10)	0.9301(6)	0.931(2)
$\bar{B}''$	0.9680(14)	0.9675(10)	0.9675(10)	0.9490(6)	0.951(2)
$\Delta_J''\times10^4$	1.4(2)	1.2(1)	1.2(1)	1.27(7)	1.1(8)
$\Delta_{JK}''\times10^4$	⋯	⋯	1.4(74)	−5.7(10)	5.5(10)
A'				75.037(7)	
B'	⋯	1.0068(10)	1.0080(10)	0.9882(6)	
C'	⋯	0.9676(10)	0.9689(10)	0.9498(6)	
$\bar{B}'$	0.9879(14)	0.9872(10)	0.9885(10)	0.9690(6)	
$\Delta_J'\times10^4$	1.1(2)	1.2(1)	1.1(1)	1.20(7)	
$\Delta_{JK}'\times10^4$	⋯	⋯	−12.8(74)	−6.4(10)	
ΔA[a]	⋯	⋯	5.71(1)	5.78(1)	
ν_0[b]	4095.24	4089.50(1)	4095.23(1)	4098.98(1)	
rms$\times10^3$	0.06	1.6	7.3	3.0	
R_{eff}''/Å			3.035	3.065	
R_{eff}'/Å			3.005	3.031	

[a]$\Delta A=A'-A''$.
[b]Subband origins are given for the K_a=0-0 and K_a=1-1 subbands.

sible to deduce both *R* and *r* from the *B* and *C* rotational constants because the inertial defect $\Delta=1/C-1/B-1/A$ is zero. Assuming for the moment that Al^+-H_2 is rigid and taking the experimental values for B'' and C'' (Table III) one finds $A''=24.4\ cm^{-1}$, corresponding to a vibrationally averaged H–H separation of 1.17 Å. This would represent an enormous 0.42 Å increase in the H–H bond length from the free H_2 molecule value ($\langle r\rangle=0.75$ Å) that is unlikely to be caused by the relatively weak interaction with an Al^+ ion (Table I). The more likely alternative to large distortion of the H_2 subunit is that the effective molecular parameters are influenced by the large amplitude bending/hindered rotation of the H_2 subunit. As noted by Nesbitt and co-workers,[41,46] the unquenched hindered internal rotation tends to exaggerate the asymmetry splitting and consequently *B*-*C*, leading to a nonzero inertial defect. The effect increases as the hindering barrier for internal rotation decreases. A similar, though less pronounced effect was found for the Li^+-H_2 and Li^+-D_2 complexes.[22,23]

Calculations based on the CCSD(T) PES supports this explanation; fits to the calculated rovibrational energies in terms of a Watson *A*-reduced Hamiltonian also give rotational constants that are not directly relatable to a rigid structure for the complex. For example, using the theoretical B'' and C'' constants (2D results from Table IV) and assuming a zero inertial defect one derives $A''=23.8\ cm^{-1}$. This is much less than the A'' value found by fitting directly the calculated rovibrational energies ($80.8\ cm^{-1}$) which is, in turn, larger than the rotational constant of the bare H_2 molecule ($59.34\ cm^{-1}$).

D. Intermolecular modes

No bands associated with excitation of the stretching or bending intermolecular modes were observed experimentally. Harmonic frequencies for the intermolecular stretch vibration estimated using the *B* and *D* constants for the ground and excited states are $\omega_s''=160\pm20\ cm^{-1}$ and $\omega_s'=190\pm20\ cm^{-1}$, respectively. These estimations are consistent with the results of the rovibrational calculations. Calculated frequencies (2D) for the intermolecular stretch and bend modes are $\nu_s''=152.9\ cm^{-1}$ and $\nu_b''=282.8\ cm^{-1}$. Excitation of the H_2 subunit leads to a stiffening of the intermolecular bond so that both intermolecular modes increase slightly in frequency ($\nu_s'=162.9\ cm^{-1}$ and $\nu_b'=287.8\ cm^{-1}$).

The calculations reveal that among the combination bands, $\nu_{HH}+\nu_s$ (predicted at $4324\ cm^{-1}$) should have the largest intensity, although it is still 40 times weaker than the ν_{HH} fundamental transition. Nevertheless, with sufficient IR power $\nu_{HH}+\nu_s$ should be detectable using IR photofragmentation, as should $\nu_{HH}+\nu_b$ (predicted at $4449\ cm^{-1}$). The $\nu_{HH}+\nu_s\leftarrow\nu_s$ and $\nu_{HH}+\nu_b\leftarrow\nu_b$ hot band transitions (predicted to occur 5–10 cm^{-1} above the ν_{HH} transition) have transition moments comparable to that of the fundamental ν_{HH} band. Their absence in the spectrum can be attributed to the low thermal population of the ν_s and ν_b levels.

E. Ground/excited state changes and vibrational redshift

The center for the ν_{HH} band occurs at $4095.2\ cm^{-1}$, a redshift of $66.0\ cm^{-1}$ from the $Q_1(0)$ transition of the free H_2 molecule ($4161.2\ cm^{-1}$; Ref. 47). The relative redshift

$\Delta\nu_{HH}/\nu_{HH}$ for Al^+-H_2 is 1.6%, somewhat less than for Li^+-H_2 and Li^+-D_2 (2.6% in both cases) and other cation-dihydrogen complexes [e.g., $\Delta\nu/\nu=2.8\%$ for $H_2-H_3O^+$,[48] and 2.3% for H_2-HCO^+ Ref. 42]. The comparatively small redshift for Al^+-H_2 emphasizes the fragility of the intermolecular $Al^+\cdots H_2$ bond ($D_0=470\pm50$ cm^{-1}; Ref. 9) compared to other charged complexes containing dihydrogen.

If the H–H stretch mode is considered effectively decoupled from the lower frequency intermolecular motions, as assumed in the 2D rovibrational calculations, the redshift can be interpreted as the difference between the intermolecular binding energies of Al^+ interacting with H_2 in the $n_{HH}=0$ and $n_{HH}=1$ states. From this perspective the effective $Al^+-H_2(n_{HH}=1)$ dissociation energy (D_0') exceeds the $Al^+-H_2(n_{HH}=0)$ dissociation energy (D_0'') by 66 cm^{-1}. The enhanced upper state interaction can be explained as a consequence of enhancements to the charge-quadrupole and charge-induced-dipole induction interactions following from 10% increases in the quadrupole moment and polarizability of H_2.[49] The same behavior follows from analysis of the *ab initio* PES (see Sec. IV A); the redshift obtained from the 2D rovibrational calculations (62.2 cm^{-1}) is in good agreement with the measured value with the small discrepancy ($\sim$3.8 cm^{-1}) being manifested as a systematic difference between the experimental and calculated transition energies listed in Table III.

F. Vibrational predissociation dynamics

The observed transitions access quasibound $n_{HH}=1$ levels that are coupled to the $Al^+ + H_2(n_{HH}=0)$ continuum. In principle, the widths of the individual rovibrational lines, which slightly exceed the IR bandwidth, provide information on the vibrational predissociation rate. The more intense $K_a=1$-1 lines were used to estimate the contribution due to lifetime broadening. Fitting a Voigt profile to the lines, with the full width at half maximum of the Gaussian component fixed to 0.017 cm^{-1} (the bandwidth of the OPO IR radiation), gives a Lorentzian component having a width $(2\pm1)\times10^{-2}$ cm^{-1} that is apparently independent of J'. The width of the Lorentzian component corresponds to an upper state lifetime of $\tau_{up}=265$ ps, somewhat longer than the values estimated for Li^+-H_2 ($\tau_{up}=53$ ps) and Li^+-D_2 ($\tau_{up}=150$ ps), perhaps reflecting a weaker coupling between the H–H stretch mode and intermolecular modes for the Al^+-H_2 system. Note that line profiles can be affected by power broadening so that the predissociation lifetimes should be regarded as lower limits. However, it should be remarked that using the same instrument we have observed narrower, laser-limited transitions for the Br^--D_2 and I^--D_2 anion complexes.[50,51]

V. CONCLUSIONS

The main outcomes and conclusions of this work can be summarized as follows.

(1) The Al^+-H_2 complex possesses a rotationally resolved H–H stretch band redshifted by 66.0 cm^{-1} from the stretch fundamental of the free H_2 diatomic molecule.
(2) The Al^+-H_2 complex has a T-shaped equilibrium structure with a vibrationally averaged intermolecular separation of 3.03 Å, decreasing by 0.03 Å when the H_2 subunit is vibrationally excited.
(3) A 265 ps lower limit for the predissociation lifetime for $Al^+-H_2(n_{HH}=1)$ is estimated from rovibrational line broadening.
(4) A new three-dimensional potential energy surface for Al^+-H_2 has been calculated at the CCSD(T) level of theory. Using the PES, effective dissociation energies of 469.4 and 506.4 cm^{-1} are predicted for Al^+-H_2 (para) and Al^+-H_2 (ortho), respectively, in very good agreement with experimental binding energy measurements ($D_0=470\pm50$ cm^{-1}; Ref. 9).
(5) Spectroscopic properties of Al^+-H_2 are well captured by the new PES. The calculations predict the H–H stretch frequency to within 3.75 cm^{-1}, the *B* and *C* rotational constants to within $\sim$2%, and the *relative* positions of the $K_a=0$-0, 1-1, and 2-2 subband origins to within 0.1 cm^{-1}. Calculations based on the PES also correctly predict that the intermolecular bond contracts by 0.03 Å when the H_2 subunit is vibrationally excited.
(6) A slight overestimation of the vibrationally averaged intermolecular separation (by 0.03 Å) may be a consequence of the Boys-Bernardi counterpoise correction overcompensating for BSSE.

ACKNOWLEDGMENTS

The authors are grateful to the Australian Research Council, the University of Melbourne, and the Russian Basic Research Fund (Project No. 05-03-32173) for financial support. One of the authors (J.K.) would also like to acknowledge financial support from the U.S. National Science Foundation under Grant No. CHE-0413743 to Professor Millard H. Alexander.

[1] J. M. Lisy, Int. Rev. Phys. Chem. **16**, 267 (1997).
[2] T. D. Vaden, C. J. Weinheimer, and J. M. Lisy, J. Chem. Phys. **121**, 3102 (2004).
[3] T. D. Vaden, J. M. Lisy, P. D. Carnegie, E. D. Pillai, and M. A. Duncan, Phys. Chem. Chem. Phys. **8**, 3078 (2006).
[4] N. R. Walker, R. S. Walters, M. K. Tsai, K. D. Jordan, and M. A. Duncan, J. Phys. Chem. A **109**, 7057 (2005).
[5] N. R. Walker, R. S. Walters, and M. A. Duncan, New J. Chem. **29**, 1495 (2005).
[6] T. Iino, K. Ohashi, Y. Mune, Y. Inokuchi, K. Judai, N. Nishi, and H. Sekiya, Chem. Phys. Lett. **427**, 24 (2006).
[7] Y. Inokuchi, K. Ohshimo, F. Misaizu, and N. Nishi, Chem. Phys. Lett. **390**, 140 (2004).
[8] Y. Mune, K. Ohashi, T. Iino, Y. Inokuchi, K. Judai, N. Nishi, and H. Sekiya, Chem. Phys. Lett. **419**, 201 (2006).
[9] P. R. Kemper, J. Bushnell, M. T. Bowers, and G. I. Gellene, J. Phys. Chem. **102**, 8590 (1998).
[10] S. B. Sharp, B. Lemoine, and G. I. Gellene, J. Phys. Chem. A **103**, 8309 (1999).
[11] G. Rasul, G. K. S. Prakash, and G. A. Olah, J. Phys. Chem. A **104**, 2284 (2000).
[12] P. R. Kemper, J. E. Bushnell, P. Weis, and M. T. Bowers, J. Am. Chem. Soc. **120**, 7577 (1998).
[13] S. B. Sharp and G. I. Gellene, J. Am. Chem. Soc. **120**, 7585 (1998).
[14] P. B. Armentrout, Int. Rev. Phys. Chem. **9**, 115 (1990).
[15] M. R. Salazar, J. Chem. Phys. **121**, 6874 (2004).
[16] R. Bell and J. Simons, J. Phys. Chem. A **103**, 539 (1999).

[17] M. R. Chacontaylor and J. Simons, Theor. Chim. Acta **90**, 357 (1995).
[18] M. Gutowski, M. Roberson, J. Rusho, J. Nichols, and J. Simons, J. Chem. Phys. **99**, 2601 (1993).
[19] A. A. Buchachenko, T. A. Grinev, J. Kłos, E. J. Bieske, M. M. Szczęśniak, and G. Chałasiński, J. Chem. Phys. **119**, 12931 (2003).
[20] R. L. Wilson, Z. M. Loh, D. A. Wild, E. J. Bieske, and A. A. Buchachenko, J. Chem. Phys. **121**, 2085 (2004).
[21] T. A. Grinev, A. A. Buchachenko, J. Kłos, and E. J. Bieske, J. Chem. Phys. **125**, 114313 (2006).
[22] C. Thompson, C. Emmeluth, B. Poad, G. Weddle, and E. Bieske, J. Chem. Phys. **125**, 044310 (2006).
[23] C. Emmeluth, B. Poad, C. Thompson, G. Weddle, and E. Bieske, J. Chem. Phys. **126**, 204309 (2007).
[24] I. Røeggen, H. Skullerud, T. Løvaas, and D. K. Dysthe, J. Phys. B **35**, 1707 (2002).
[25] V. P. Bulychev, K. M. Bulanin, and M. O. Bulanin, Opt. Spectrosc. **96**, 205 (2004).
[26] C. Sanz, E. Bodo, and F. A. Gianturco, Chem. Phys. **314**, 135 (2005).
[27] W. P. Kraemer and V. Špirko, Chem. Phys. **330**, 190 (2006).
[28] D. A. Wild and E. J. Bieske, Int. Rev. Phys. Chem. **22**, 129 (2003).
[29] H.-J. Werner, P. J. Knowles, R. Lindh *et al.*, MOLPRO, version 2002.6, a package of *ab initio* programs, 2006; URL: http://www.molpro.net/
[30] R. A. Kendall, T. H. Dunning, Jr., and R. J. Harrison, J. Chem. Phys. **96**, 6796 (1992).
[31] D. E. Woon and T. H. Dunning, Jr., J. Chem. Phys. **100**, 2975 (1994).
[32] S. M. Cybulski and R. R. Toczylowski, J. Chem. Phys. **111**, 10520 (1999).
[33] C. Hampel, K. Peterson, and H.-J. Werner, Chem. Phys. Lett. **190**, 1 (1992).
[34] J. D. Watts, J. Gauss, and R. J. Bartlett, J. Chem. Phys. **98**, 8718 (1993).
[35] P. J. Knowles and H.-J. Werner, Chem. Phys. Lett. **115**, 259 (1985).
[36] S. Boys and F. Bernardi, Mol. Phys. **19**, 553 (1970).
[37] See EPAPS Document No. E-JCPSA6-127-022735 for the Al^+-H_2 PES and the calculated energy levels. This document can be reached through a direct link in the online article's HTML reference section or via the EPAPS homepage (http://www.aip.org./pubservs/epaps.html).
[38] J. Tennyson, Comput. Phys. Rep. **4**, 1 (1986).
[39] G. Delgado-Barrio and J. A. Beswick, *Structure and Dynamics of Non-Rigid Molecular Systems* (Kluwer, Dordrecht, 1994), p. 203.
[40] B. P. Reid, K. C. Janda, and N. Halberstadt, J. Phys. Chem. **92**, 587 (1988).
[41] C. Lovejoy, D. Nelson, and D. J. Nesbitt, J. Chem. Phys. **87**, 5621 (1987).
[42] E. J. Bieske, S. A. Nizkorodov, F. R. Bennett, and J. P. Maier, J. Chem. Phys. **102**, 5152 (1995).
[43] D. A. Wild, P. S. Weiser, E. J. Bieske, and A. Zehnacker, J. Chem. Phys. **115**, 824 (2001).
[44] T. A. Grinev, A. A. Buchachenko, and R. V. Krems, ChemPhysChem **8**, 815 (2007).
[45] K. P. Huber and G. Herzberg, *Constants of Diatomic Molecules*, Molecular Spectra and Molecular Structure Vol. 4 (van Nostrand Reinhold, New York, 1979).
[46] D. J. Nesbitt and R. Naaman, J. Chem. Phys. **91**, 3801 (1989).
[47] S. L. Bragg, J. W. Brault, and W. H. Smith, Astrophys. J. **263**, 999 (1982).
[48] M. Okumura, L. I. Yeh, J. D. Myers, and Y. T. Lee, J. Phys. Chem. **94**, 3416 (1990).
[49] L. Wolniewicz, J. Chem. Phys. **45**, 515 (1966).
[50] D. A. Wild, P. S. Weiser, and E. J. Bieske, J. Chem. Phys. **115**, 6394 (2001).
[51] D. A. Wild and E. J. Bieske, J. Chem. Phys. **121**, 12276 (2004).